JPEDAV (2004) 25:507-514
DOI: 10.1361/15477020421025
1547-7037/$19.00 ©ASM International

Phase Relations in the Nb-Pd-Hf-Al System

A. Misra, G. Ghosh, and G.B. Olson

(Submitted December 14, 2003; in revised form September 23, 2004)

In support of computational design of coherent aluminide strengthened Nb alloys, the phase equilibria in a series of six Nb-Pd-Hf-Al alloys were investigated using scanning electron microscopy (SEM) and x-ray diffraction (XRD). All alloys were heat treated at 1200 °C for 200 h, while three alloys were also heat treated at 1500 °C for 200 h. Three-phase equilibria and two-phase equilibria were observed in two alloys at both temperatures. Two more alloys also exhibited three-phase equilibria at 1200 °C, while one alloy exhibited two-phase equilibria at 1200 °C. A final alloy revealed four-phase equilibria at both temperatures, confirming the presence of a unique tie-tetrahedron in the Nb-Pd-Hf-Al system. Based on the characterization of phases by SEM and XRD, the Nb-Pd-Hf-Al partial phase diagram at 1200 °C has been constructed. Such phase diagrams provide the basis for designing precipitation-strengthened Nb-based superalloys.

1. Introduction

Currently, Ni-based superalloys are the materials of choice for high-temperature turbine blade applications. However, the efficiency of the turbine blades is limited by their operating temperature, which in turn is limited by the melting point of Ni-based superalloys. To increase the operating temperature of turbine blades to around 1300 °C, Nb-based superalloys are being considered as a potential replacement. Niobium has a high melting point (2467 °C) and low density (Ref 1), making it an attractive candidate for the replacement of nickel. However, niobium has very poor oxidation resistance at high temperatures (Ref 2) and limited creep strength (Ref 3).

A multi-institutional project is underway under the Air Force-Materials Engineering for Affordable New Systems (AF-MEANS) initiative to design a high-strength, oxidation-resistant Nb-based superalloy. The authors' systems engineering approach (Ref 4) to design Nb-based superalloys is represented by Fig. 1. It summarizes the processing-structure-property-performance links governing the behavior of a multilevel-structured coated Nb-based superalloy system. While the total system integrates compatible thermal barrier and bond-coat subsystems, the authors' initial research focused on predictive design of the underlying precipitation-strengthened alloy. The specific tools used in this effort explore the limits of modern quantum engineering methods based on total energy calculations.

The high strength in the alloy may be obtained by the dispersion of coherent ordered body-centered-cubic (bcc)-type aluminides (such as the *B*2 and Heusler phases) in a bcc Nb matrix phase. In the scope of this research project, the aluminides identified as strengthening phase candidates are *B*2 PdAl and Heusler Pd_2HfAl. To design alloys with (Nb) as the matrix phase and PdAl and Pd_2HfAl as the precipitates, accurate knowledge of the Nb-Pd-Hf-Al quaternary phase diagram is required. A previous study reported preliminary results on phase equilibria in the Nb-Pd-Hf-Al system (Ref 5). This paper reports a more extensive composition analysis of phases in several prototype Nb-Pd-Hf-Al alloys. The measured phase relations enabled construction of the partial Nb-Pd-Hf-Al quaternary phase diagrams at 1200 °C, defining phase field limits of importance to aluminide-strengthened alloys.

A. Misra, G. Ghosh, and **G.B. Olson,** Department of Materials Science and Engineering, Robert R. McCormick School of Engineering and Applied Science, Northwestern University, 2220 Campus Dr., Evanston, IL 60208-3108. Contact e-mail: g-ghosh@northwestern.edu.

2. Experimental Procedure

In this study, six Nb-Pd-Hf-Al alloys were prepared for phase equilibria investigation. The alloys were designated 995, 996, 40Nb, 50Nb, 60Nb, and 80Nb. Alloys 995 and 996 were prepared to have the nominal compositions (in atomic percent) of 60Nb-20Pd-10Hf-10Al (alloy 995) and 40Nb-30Pd-15Hf-15Al (alloy 996). The experimental details of the processing of alloys 995 and 996 were reported earlier (Ref 5).

Alloys 40Nb, 50Nb, 60Nb, and 80Nb were prepared to have the nominal compositions (in atomic percent) of 40Nb-30Pd-18Hf-12Al, 50Nb-27Pd-1.5Hf-21.5Al, 60Nb-20Pd-10Hf-10Al, and 80Nb-10Pd-5Hf-5Al, respectively. It is important to note that, although alloy 995 and alloy 60Nb have the same nominal composition, the bulk composition of alloy 995 turned out to be significantly different from the intended nominal composition due to processing issues, as discussed previously (Ref 5). The compositions of alloys 40Nb, 50Nb, 60Nb, and 80Nb were chosen based on the previous phase relations measured in alloys 995 and 996 as well as the Hf-Pd binary phase diagram (Ref 6) and were expected to give further information about the phase fields surrounding the (Nb)-Pd_2HfAl and (Nb)-PdAl two-phase fields.

The starting materials were pure elements of the following purity: Nb 99.8%, Pd 99.95%, Hf 99.9%, and Al 99.999%. These were weighed to the desired amounts on a

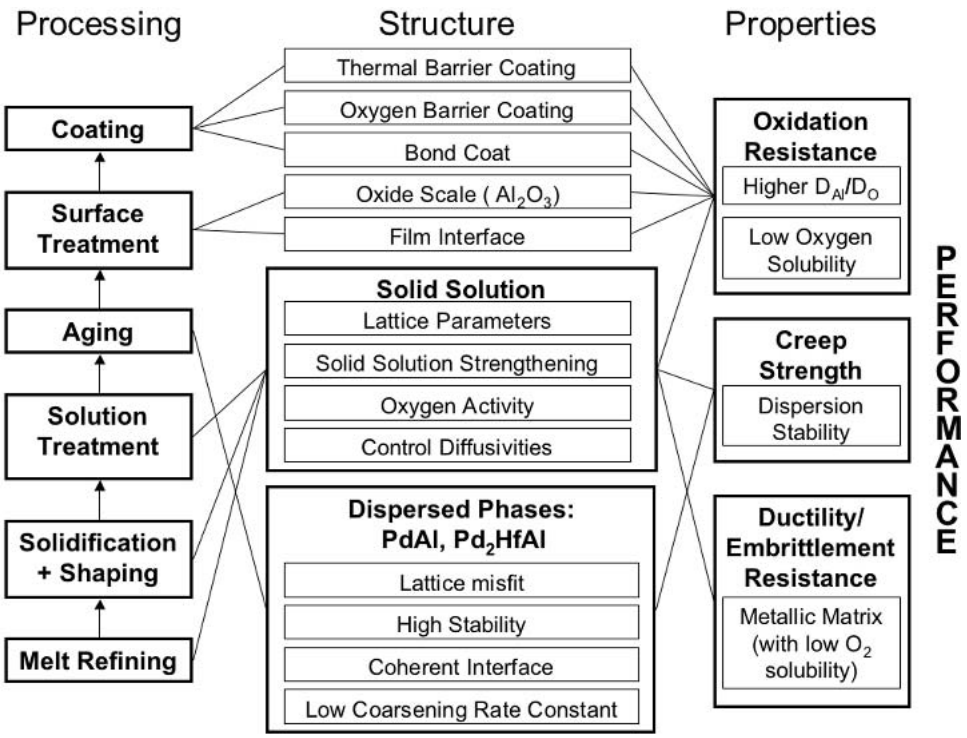

Fig. 1 Systems design chart for niobium superalloys

Table 1 Crystallographic data of the observed phases

Phase	Pearson symbol	Space group (No.)	Lattice parameter at 25 °C, nm	Comments
(αHf)	*hP*2	$P6_3/mmc$ (194)	a = 0.31946 (Ref 9) c = 0.50511	Pure αHf
(Nb)	*cI*2	$Im\bar{3}m$ (229)	a = 0.33007 (Ref 9)	Pure Nb
PdAl	*cP*2	$Pm\bar{3}m$ (221)	a = 0.30532 (Ref 10)	Stoichiometric
Pd_2HfAl	*cF*16	$Fm\bar{3}m$ (225)	a = 0.6367 (Ref 11)	Stoichiometric
Pd_3Hf	*hP*16	$P6_3/mmc$ (195)	a = 0.5595 (Ref 6) c = 0.9192	Stoichiometric
Pd_2Hf	*tI*6	*I*4/*mmm* (139)	a = 0.3390 (Ref 6) c = 0.8658	Stoichiometric
PdHf	…	…	…	Crystal structure not known

Mettler H80 scale (Mettler-Toledo, Inc., Columbus, OH) with four decimal place accuracy. The alloys were made by arc melting in an inert argon atmosphere and were flipped and remelted at least ten times to achieve homogeneity.

Samples were cut from the ingots and were then heat-treated at 1200 and 1500 °C (for alloys 995, 996, and 40Nb) for 200 h each. Samples for the 1200 °C heat treatment were vacuum encapsulated in a quartz tube with tantalum foil to getter residual oxygen. The 1500 °C heat treatment was performed at the University of Wisconsin at Madison in a high-purity argon atmosphere furnace.

A Hitachi 4500 (Hitachi Ltd., Tokyo, Japan) scanning electron microscope (SEM) having a cold field emission gun was used for microstructural characterization on alloys 995 and 996. Standards-based composition analysis on all samples and microstructural characterization on alloys 40Nb, 50Nb, 60Nb, and 80Nb was carried out on a Hitachi 3500 SEM having a tungsten filament and fitted with a PGT (Princeton Gamma-Tech, Princeton, NJ) energy dispersive spectrometer (EDS) and PGT-IMIX (Integrated Microanalyzer for Imaging and X-ray) software and ZAF (Z: atomic number, A: absorption, F: fluorescence) parameter database. A 20 kV accelerating voltage was used for EDS analysis. X-ray diffraction (XRD) was performed on a Scintag XDS 2000 diffractometer with a Cu Kα source. The diffraction patterns were then analyzed using MacDiff software (Ref 7) to precisely determine the peak positions, assuming split pseudo-Voigt shape of the peaks. Lattice parameter values were obtained from the peak positions and, in the case of (Nb), Pd_2HfAl, and *B*2 PdAl; these were plotted

against the Nelson-Riley function (Ref 8) to obtain precise lattice parameters.

3. Results

3.1 Phase Equilibria

The crystallographic data of observed phases in model alloys under study are summarized in Table 1. A detailed description of the different phase equilibria present in alloys 995 and 996 and the measured phase compositions and lattice parameters has been reported earlier (Ref 5). Nevertheless, representative micrographs of alloys 995 and 996 heat treated at 1200 °C are shown in Fig. 2 and 3, respectively. Figure 2 shows a three-phase equilibrium among (Nb), Pd_2HfAl, and Pd_3Hf, and Fig. 3 shows a three-phase equilibrium among (Nb), PdAl, and (αHf). As mentioned in the previous publication (Ref 5), alloy 996 heat treated at 1200 °C showed the presence of four regions in the sample. Three three-phase regions [(Nb) + (αHf) + PdAl, (Nb) + PdAl + Pd_3Hf, and (Nb) + Pd_2HfAl + Pd_3Hf] and one two-phase region [(Nb) + Pd_2HfAl] were observed in the sample. This was due to compositional inhomogeneity in the sample that was not intentional, but was a result of macrosegregation occurring in the sample after cold crucible induction melting. Nevertheless, the nonuniform sample yielded important compositional information about the different tie-triangles existing in this system.

The overall compositions of alloys 40Nb, 50Nb, 60Nb, and 80Nb were measured using EDS to gage the extent of their deviation from the intended alloy compositions. The measured overall compositions of the alloys are summarized in Table 2. It can be seen in Table 2 that the deviations from the intended nominal compositions are of the order of 1 at.%, although in some cases the deviations are more than 2 at.%. This is mostly due to the disparity of the melting points of the components (especially Nb and Al) in the system and the preferential evaporation of Al during arc melting; a problem also experienced by other researchers (Ref 12).

Alloy 40Nb showed the presence of four phases after both 1200 and 1500 °C heat treatments. Representative micrographs are shown in Fig. 4(a) and (b). The phases are (Nb), Pd_2HfAl, PdHf (identified only on the basis of composition), and a fourth phase that has a composition close to both Pd_4Hf_3 and Pd_2Hf. The assesed Hf-Pd binary phase diagram (Ref 6) shows that Pd_2Hf is only stable above 1370 °C. However, Kuznetsov et al. found that Pd_2Hf exists even after annealing at 1000 °C (Ref 13). Also, they could not confirm the existence of Pd_4Hf_3. The structures of PdHf and Pd_4Hf_3 are not known, whereas Pd_2Hf is known to have a tetragonal structure of space group *I*4/*mmm* (Ref 6). The XRD spectrum of the 40Nb heat treated samples revealed strong peaks at $2\theta = 41.136°$ (for the 1200 °C sample) and 41.239° (for the 1500 °C sample), which are very close to the maximum intensity (103) diffraction peak for Pd_2Hf (41.106°) (Ref 14). Based on the Hf content and XRD results, the authors conclude that the fourth phase is Pd_2Hf with a significant amount of Al residing primarily on the Pd sublattice. The compositions of the phases and the lattice parameters of (Nb) and Pd_2HfAl phases in alloy 40Nb at both heat treatments are summarized in Table 3.

Alloy 50Nb exhibited two-phase equilibria at 1200 °C. The phases present in the alloy were (Nb) and *B*2 PdAl. The overall Hf content in the alloy was very low, and the alloy was intended to lie in the above two-phase field. The com-

Table 2 Measured overall compositions of the alloys 40Nb, 50Nb, 60Nb, and 80Nb

	Composition, at.%			
Alloy	Nb	Pd	Hf	Al
40Nb	38.3 ± 0.4	31.6 ± 0.5	15.9 ± 0.2	14.2 ± 0.4
50Nb	47.3 ± 1.1	32.0 ± 0.6	1.2 ± 0.3	19.5 ± 0.6
60Nb	62.7 ± 3.3	20.2 ± 1.8	8.6 ± 0.7	8.5 ± 0.9
80Nb	81.0 ± 2.7	10.8 ± 1.9	4.2 ± 0.8	4.0 ± 0.4

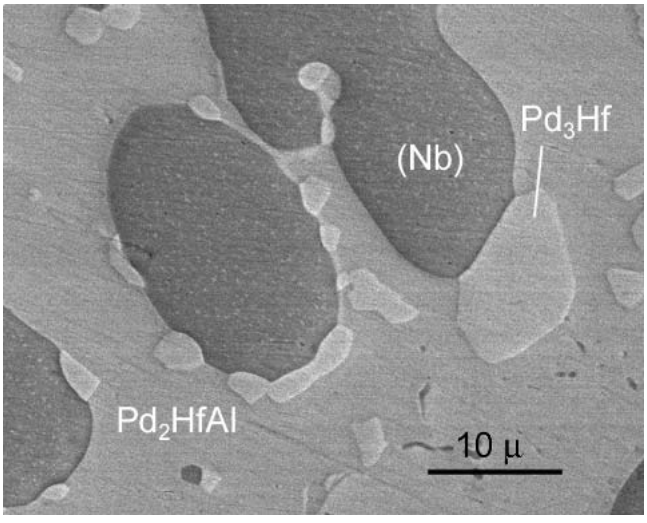

Fig. 2 Microstructure of alloy 995 heat treated at 1200 °C, showing the presence of three phases

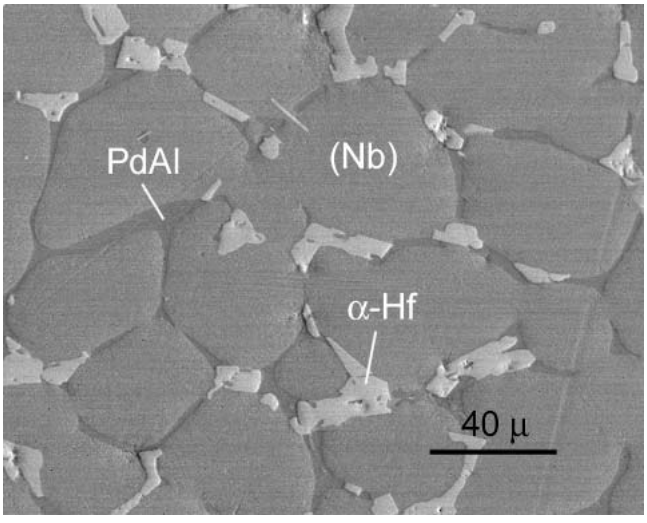

Fig. 3 Microstructure of alloy 996 heat treated at 1200 °C, showing the presence of three phases

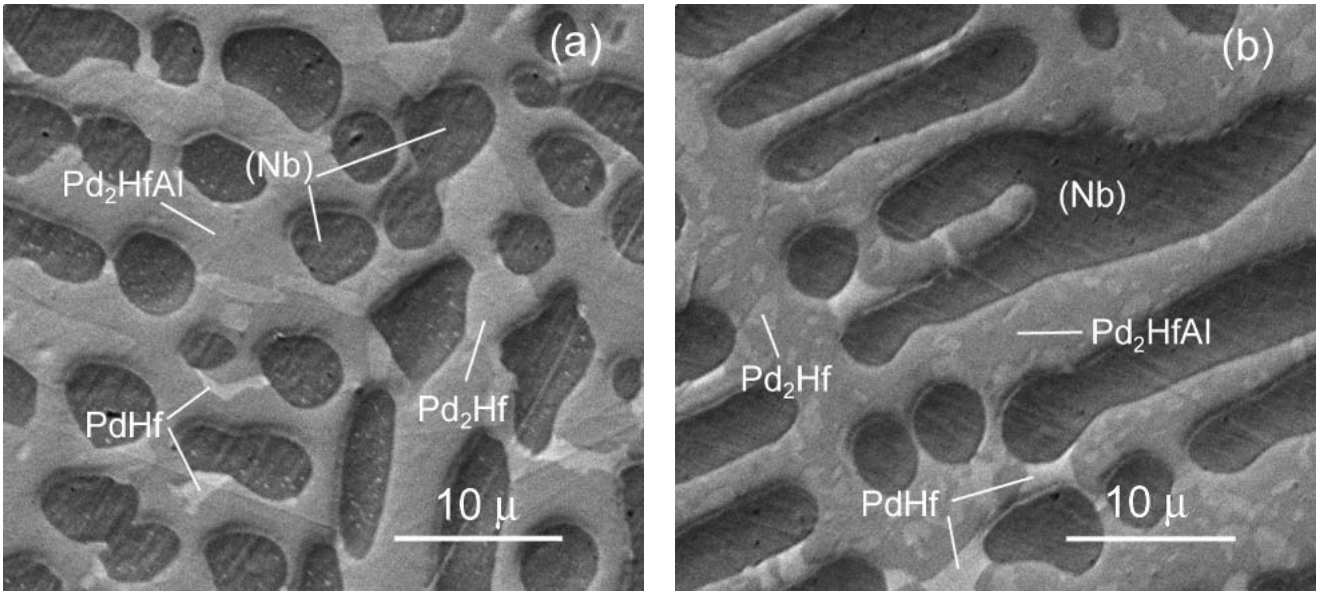

Fig. 4 Microstructure of alloy 40Nb showing the presence of four phases. **(a)** Heat treated at 1200 °C. **(b)** Heat treated at 1500 °C

Table 3 Measured composition of the phases and their lattice parameters in alloy 40Nb

Heat treatment	Phases	Composition, at.%				Lattice parameter, nm
		Nb	Pd	Hf	Al	
1200 °C, 200 h	(Nb)	86.0 ± 2.5	4.1 ± 1.4	5.5 ± 0.5	4.4 ± 0.8	a = 0.33060 ± 0.00022
	Pd_2HfAl	0.4 ± 0.2	49.3 ± 0.9	24.0 ± 0.6	26.3 ± 0.9	a = 0.63973 ± 0.00005
	Pd_2Hf	1.5 ± 1.5	56.0 ± 1.0	30.5 ± 0.5	12.0 ± 1.1	…
	PdHf	2.0 ± 1.2	49.1 ± 1.5	38.0 ± 0.7	10.9 ± 2.1	…
1500 °C, 200 h	(Nb)	89.8 ± 1.7	3.6 ± 1.1	3.5 ± 0.5	3.1 ± 0.4	a = 0.33048 ± 0.00006
	Pd_2HfAl	1.1 ± 0.3	48.4 ± 0.8	24.8 ± 0.4	25.7 ± 0.6	a = 0.63894 ± 0.00001
	Pd_2Hf	1.3 ± 0.3	53.6 ± 1.3	31.8 ± 1.1	13.3 ± 0.5	…
	PdHf	2.3 ± 0.4	46.5 ± 1.3	41.7 ± 0.6	9.5 ± 1.3	…

Table 4 Measured composition of the phases and their lattice parameters in alloys 50Nb, 60Nb, and 80Nb heat treated at 1200 °C

Alloy	Phases	Composition, at.%				Lattice parameter, nm
		Nb	Pd	Hf	Al	
50Nb	(Nb)	84.5 ± 2.1	9.4 ± 1.0	0.2 ± 0.2	5.9 ± 1.1	a = 0.32854 ± 0.00017
	PdAl	0.2 ± 0.2	52.5 ± 0.6	2.8 ± 0.1	44.5 ± 0.5	a = 0.30749 ± 0.00016
60Nb	(Nb)	89.2 ± 1.2	5.0 ± 0.7	2.6 ± 0.4	3.2 ± 0.3	a = 0.32992 ± 0.00005
	Pd_2HfAl	0.4 ± 0.6	50.9 ± 1.0	24.0 ± 0.5	24.7 ± 1.2	a = 0.63777 ± 0.00017
	(αHf)	1.4 ± 0.6	0.1 ± 0.1	98.4 ± 0.8	0.1 ± 0.1	…
80Nb	(Nb)	91.1 ± 1.5	4.7 ± 1.0	2.0 ± 0.4	2.2 ± 0.6	a = 0.33015 ± 0.00011
	Pd_2HfAl	0.7 ± 0.3	51.9 ± 1.0	22.0 ± 0.9	25.4 ± 0.6	a = 0.63769 ± 0.00024
	Pd_2Hf	2.1 ± 1.8	59.3 ± 1.0	30.3 ± 1.9	8.3 ± 1.5	…

positions of the phases and the lattice parameters of (Nb) and PdAl phases in the alloy are summarized in Table 4. As seen in Table 4, the Hf has partitioned strongly to the PdAl phase. The measured lattice parameter of the PdAl phase in the alloy is 0.30749 nm. Ettenberg et al. reported the lattice parameter of the equiatomic PdAl phase to be 0.30532 nm and also reported that the lattice parameter of the PdAl phase decreases from its equiatomic value on either side of stoichiometry (Ref 10). Hence, the increase in lattice parameter of the PdAl phase in the alloy, from its equiatomic value, is clearly due to the dissolved Hf atoms (as the atomic volume of Hf is significantly greater than that of either Pd or Al, Ref 9). Representative microstructure of alloy 50Nb is shown in Fig. 5.

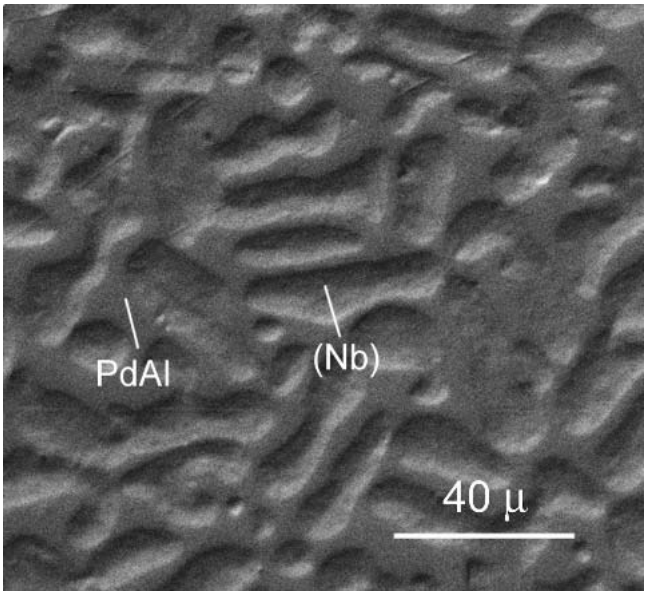

Fig. 5 Microstructure of alloy 50Nb heat treated at 1200 °C, showing the presence of two phases

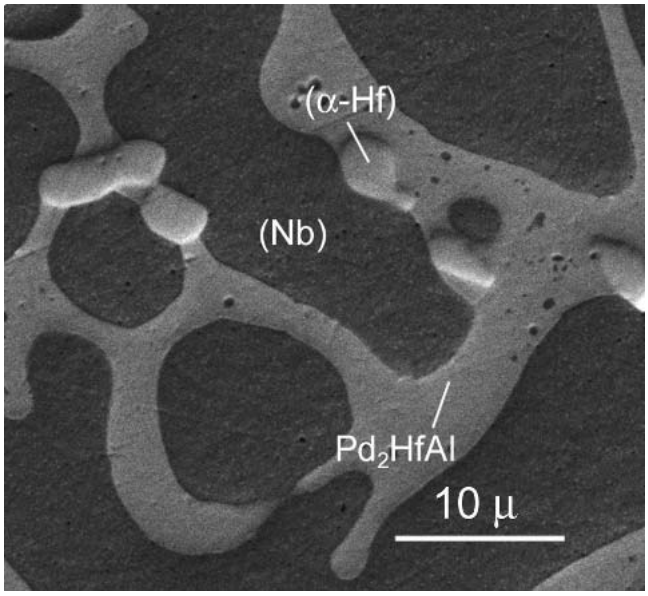

Fig. 6 Microstructure of alloy 60Nb heat treated at 1200 °C, showing the presence of three phases

Alloys 60Nb and 80Nb showed the presence of three-phase fields at 1200 °C. The phases present in alloy 60Nb are (Nb), Pd_2HfAl, and (αHf) and the phases present in alloy 80Nb are (Nb), Pd_2HfAl, and Pd_2Hf. Both the (αHf) phase in alloy 60Nb and the Pd_2Hf phase in alloy 80Nb are present in very small phase fractions, suggesting that those alloys are right on the edge of the (Nb) + Pd_2HfAl two-phase field. Representative microstructures of alloys 60Nb and 80Nb heat treated at 1200 °C are shown in Fig. 6 and 7, respectively. The compositions of the phases and the lattice parameters of (Nb) and Pd_2HfAl phases in both alloys are also summarized in Table 4.

The phase relation information obtained from all the alloys provides the basis for constructing Nb-Pd-Hf-Al partial phase diagrams. Isothermal sections of the Nb-Pd-Hf-Al phase diagram at 1200 °C can be constructed by projecting the compositions of all the phases in equilibrium with (Nb) onto the Pd-Hf-Al basal plane (Fig. 8). The phase boundaries represent the best estimate based on the available composition data. The solid circles correspond to projected data points and the open circles correspond to the reported solubility limits of the binary compounds (Ref 6, 15, 16). The numbers in parenthesis indicate the actual Nb content of the phases. The dashed lines indicate the experimental tie-lines.

Figure 8 shows three three-phase regions projected onto the Pd-Hf-Al plane. The (Nb) phase in equilibrium with the three-phase regions define three unique tie-tetrahedra in the Nb-Pd-Hf-Al system at 1200 °C (Fig. 9).

3.2 Mean Atomic Volume and Lattice Parameter of Nb-Based Solid Solution and Pd_2HfAl

In the authors' previous publication, a detailed modeling of the mean atomic volumes and lattice parameters of the Nb-based solid solution and the Pd_2HfAl phase was carried out (Ref 5). The values calculated from those models showed good agreement with the measured lattice parameters for the Nb-based solid solution and the Pd_2HfAl phase in alloys 995 and 996. In this paper, the authors seek to compare the model values with the measured lattice parameters in alloys 40Nb, 50Nb, 60Nb, and 80Nb.

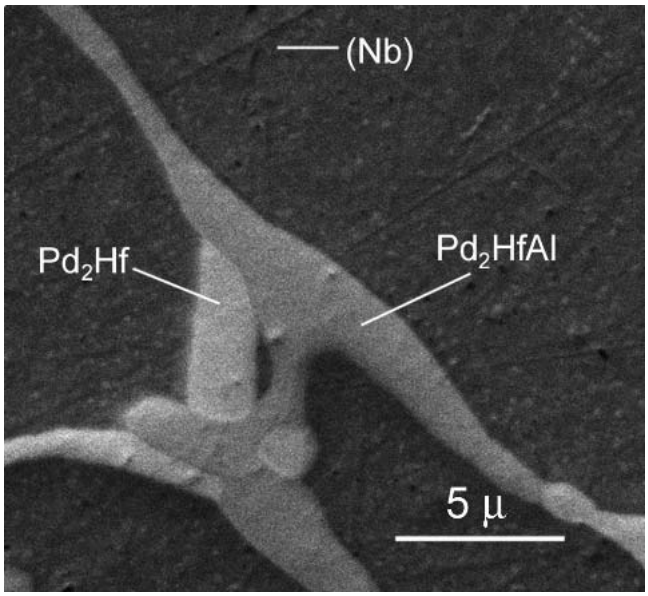

Fig. 7 Microstructure of alloy 80Nb heat treated at 1200 °C, showing the presence of three phases

The mean atomic volume of the Nb-based bcc solid solution at 25 °C can be described as

$$V_a \times 10^3\ \text{nm}^3 = 17.169\,X_{Al} + 21.815\,X_{Hf} + 17.980\,X_{Nb} + 14.815\,X_{Pd} + X_{Al}X_{Nb}[-2.8267 - 2.6218(X_{Al} - X_{Nb})] - 0.3573\,X_{Hf}X_{Nb} - 0.9695\,X_{Nb}X_{Pd} \quad \text{(Eq 1)}$$

where X_i (i = Nb, Pd, Hf, Al) is the atomic fraction of the

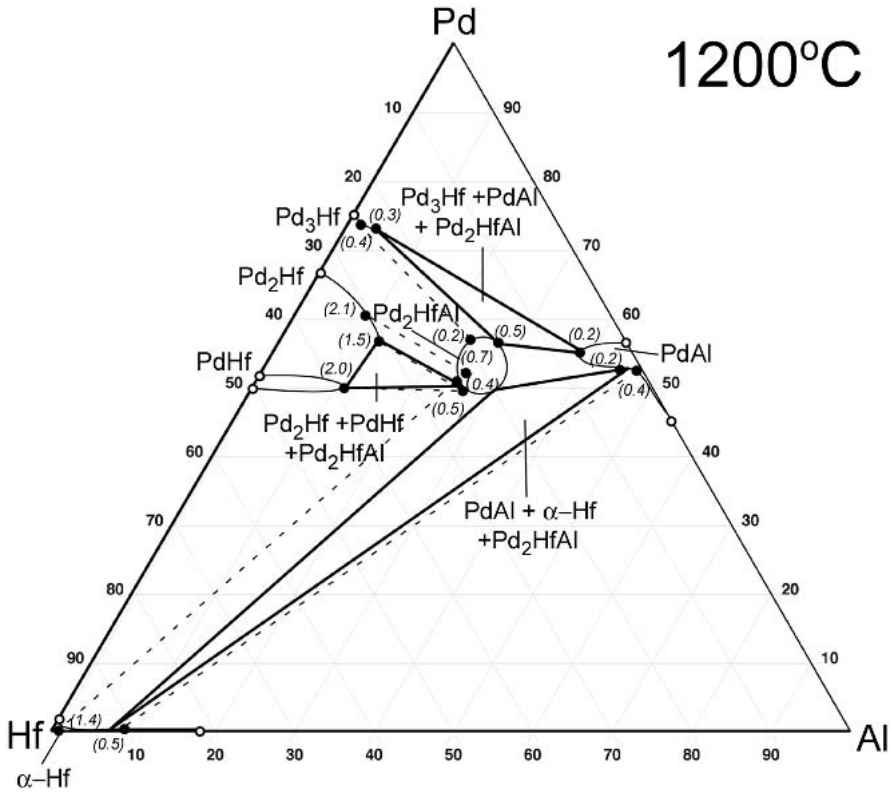

Fig. 8 Projection of Nb-Pd-Hf-Al tie-tetrahedra bases on Pd-Hf-Al plane at 1200 °C. The labeled phase fields are in equilibrium with the (Nb) phase. The numbers in the parentheses are the Nb contents of the projected phases.

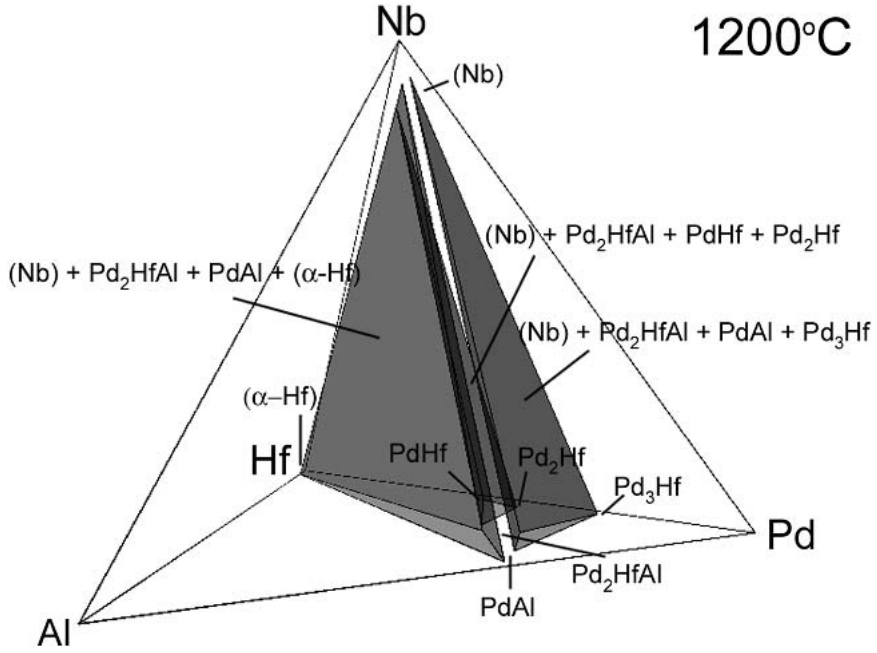

Fig. 9 Tie-tetrahedra in the Nb-Pd-Hf-Al quaternary system at 1200 °C

corresponding element (Ref 5). The lattice parameter can be obtained from the mean atomic volume by

$$a\,(\text{nm}) = \sqrt[3]{2V_a} \qquad \text{(Eq 2)}$$

The lattice parameters for the Nb solid solutions in alloys 40Nb, 50Nb, 60Nb, and 80Nb were calculated using Eq 1 and 2. The error bars for the predicted lattice parameters, related to the uncertainty of the measured compositions

Table 5 Comparison of the calculated and experimental lattice parameter (at 25 °C) of (Nb) in Nb-Pd-Hf-Al alloys

Alloy and heat treatment	*a*, nm, measured	*a*, nm, Eq 1, 2	Difference
Alloy 40Nb at 1200 °C	0.33060 ± 0.00022	0.32987 ± 0.00031	0.2%
Alloy 40Nb at 1500 °C	0.33048 ± 0.00006	0.32969 ± 0.00019	0.2%
Alloy 50Nb at 1200 °C	0.32854 ± 0.00017	0.32727 ± 0.00031	0.4%
Alloy 60Nb at 1200 °C	0.32992 ± 0.00005	0.32913 ± 0.00010	0.2%
Alloy 80Nb at 1200 °C	0.33015 ± 0.00011	0.32914 ± 0.00021	0.3%

Table 6 Comparison of the calculated and experimental lattice parameters for Pd_2HfAl

Alloy and heat treatment	*a*, nm, measured	*a*, nm, Eq 3	Difference
Alloy 40Nb at 1200 °C	0.63973 ± 0.00005	0.63598 ± 0.00050	0.6%
Alloy 40Nb at 1500 °C	0.63894 ± 0.00001	0.63700 ± 0.00042	0.3%
Alloy 60Nb at 1200 °C	0.63777 ± 0.00017	0.63613 ± 0.00062	0.3%
Alloy 80Nb at 1200 °C	0.63769 ± 0.00024	0.63457 ± 0.00082	0.5%

(Tables 3 and 4), were calculated using a standard mathematical procedure. Table 5 shows the comparison between the measured lattice parameters and the predicted values (using Eq 1 and 2) for the Nb solid solutions. As seen in Table 4, the agreement is within 0.4%, which is similar to the kind of agreement obtained earlier.

A detailed lattice parameter modeling of the Pd_2HfAl phase has also been carried out previously to account for the composition dependence (Ref 5). A fundamental assumption in the model is that the atomic volume of a species is independent of the site it occupies. In this model, the lattice parameter of Pd_2HfAl is expressed as

$$a^3 = 8\sum_{j=1}^{n} y_j^{\mathrm{I}}\Omega_j^{\mathrm{L21}} + 4\sum_{j=1}^{n} y_j^{\mathrm{II}}\Omega_j^{\mathrm{L21}} + 4\sum_{j=1}^{n} y_j^{\mathrm{III}}\Omega_j^{\mathrm{L21}} \qquad \text{(Eq 3)}$$

with $\Sigma y_j^{\mathrm{I}} = \Sigma y_j^{\mathrm{II}} = \Sigma y_j^{\mathrm{III}} = 1$; y_j is the site fraction of species j, Ω_j is the atomic volume of species j, and n is the total number of each species. Equation 3 assumes a negligible amount of Nb in Pd_2HfAl, which is the situation in this case. Following a procedure discussed previously, the atomic volume of the species are derived as: $\Omega_{\mathrm{Nb}} = 0.017980$ nm^3, $\Omega_{\mathrm{Al}} = 0.014272$ nm^3, $\Omega_{\mathrm{Pd}} = 0.014737$ nm^3, and $\Omega_{\mathrm{Hf}} = 0.020780$ nm^3 (Ref 5).

The lattice parameter of Pd_2HfAl was calculated using the above atomic volumes in a similar manner as described in Ref 5. The error bars for the calculated lattice parameters, related to the uncertainty in the measured compositions, are calculated using a standard mathematical procedure. Table 6 gives a comparison between the measured and calculated lattice parameters for the Pd_2HfAl phase. As seen from Table 6, the agreement is within 0.6%.

4. Conclusions

The phase equilibria of the Nb-Pd-Hf-Al system was investigated experimentally using model alloys. The phase relations were established in samples heat treated at 1200 and at 1500 °C. The measured phase relations provide information for constructing the Nb-Pd-Hf-Al partial quaternary phase diagram at 1200 °C. Such phase diagrams provide the basis for designing precipitation-strengthened Nb-based superalloys. The separation of the three tie-tetrahedra bases in Fig. 9 defines the boundaries of the three-phase fields between them. The tie-tetrahedron (Nb) + Pd_2HfAl + Pd_2Hf + PdHf is experimentally verified both at 1200 and 1500 °C. The separation between the three-phase fields in turn defines the limit of the Nb-Pd_2HfAl two-phase field for designing precipitation-strengthened two-phase alloys. Similarly, the width of the Nb-PdAl-Pd_2HfAl three-phase field defines the limits for designing precipitation-strengthened three-phase alloys. The lattice parameter models for the bcc phase and the Pd_2HfAl phase were compared against the new data to check their validity. The good agreement between the predicted lattice parameters and measured lattice parameters validates the accuracy of the authors' models.

Acknowledgments

This work was financially supported by the AFOSR-MEANS Program (F49620-01-1-0529) and Reference Metals Company, Inc., Bridgeville, PA. The authors also thank Professor John Perepezko, University of Wisconsin, Madison, for help in heat treating the alloys at 1500 °C.

References

1. E.A. Brandes and G.B. Brook, *Smithells Metals Reference Book,* 7th ed., Buterworth-Heinemann, 1992, p 2
2. C. Bouillet, D. Ciosmak, M. Lallemant, C. Laruelle, and J.J. Heizmann, Oxidation of Niobium Sheets at High Temperature, *Solid State Ionics,* Vol 101, 1997, p 819-824
3. M.J. Davidson, M. Biberger, and A.K. Mukherjee, Creep of Niobium and Solid-Solution Strengthened Nb-1wt.Percent-Zr, *Scr. Metall. Mater.,* Vol 27, 1992, p 1829-1834
4. G.B. Olson, Computational Design of Hierarchically Structured Materials, *Science,* Vol 277, 1997, p 1237-1242
5. A. Misra, R. Bishop, G. Ghosh, and G.B. Olson, Phase Equi-

libria in Prototype Nb-Pd-Hd-Al Alloys, *Metall. Mater. Trans.,* Vol 34A, 2003, p 1771-1781
6. S.N. Tripathi and S.R. Bharadwaj, The Hf-Pd (Hafnium-Palladium) System, *J. Phase Equilibria,* Vol 16, 1995, p 527-531
7. http://servermac.geologie.uni-frankfurt.de/MacDiff.html
8. B.D. Cullity, *Elements of X-Ray Diffraction,* 2nd ed., Addison-Wesley, 1978, p 350-367
9. H. King, Crystal Structure of the Elements at 25 °C, *Bull. Alloy Phase Diagrams,* Vol 2, 1981, p 402
10. M. Ettenberg, K. Komarek, and E. Miller, Thermodynamic Properties and Ordering in PdAl, *Metall. Trans.,* Vol 2, 1971, p 1173-1181
11. R. Marazza, G. Rambaldi, and R. Ferro, Fasi Intermetalliche Ternarie, a Rapporto Stochiometrico 1:1:2, di Struttura Tipo CsCl o Tipo $AlCu_2Mn$, *Atti Della Accademia Nazioonale Dei Lincei, Classe Di Scienze Fiiche, Matematiche E Naturali, Rendiconti,* Vol 55, 1973, p 518-521 (in Italian)
12. F. Ebrahimi and J.G.L. Ruiz-Aparicio, Diffusivity in the Nb-Ti-Al Ternary Solid Solution, *J. Alloys Compd.,* Vol 245, 1996, p 1-9
13. V.N. Kuznetsov, G.P. Zhmurko, and E.M. Sokolovskaya, Phase Equilibria and Structural Stability of Intermetallics in the Pt-Pd-Hf and Pt-Pd-Zr Systems, *J. Less-Common Met.,* Vol 163, 1990, p 1-8
14. Powder Diffraction Files, 1998, JCPDS-International Centre for Diffraction Data
15. *Binary Alloy Phase Diagrams,* 2nd ed., J.L. Murray, A.J. McAlister, and D.J. Kahan, Ed., Vol 1, ASM International, 1990, p 156-157
16. *Binary Alloy Phase Diagrams,* 2nd ed., A.J. McAlister, Ed., Vol 1, ASM International, 1990, p 189-192